Nonlinear Robust Control and Observation for Aeroelastic Launch Vehicles with Propellant Slosh in a Turbulent Atmosphere

Mooij, E.; Wang, Xuerui

DOI
10.2514/6.2023-1999

Publication date
2023

Document Version
Final published version

Published in
AIAA SciTech Forum 2023

AIAA SciTech Forum
23-27 January 2023, National Harbor, MD & Online
AIAA SCITECH 2023 Forum

10.2514/6.2023-1999

Nonlinear Robust Control and Observation for Aeroelastic Launch Vehicles with Propellant Slosh in a Turbulent Atmosphere

Erwin Mooij* and Xuerui Wang†
Delft University of Technology, Faculty of Aerospace Engineering,
Kluyverweg 1, 2629 HS Delft, The Netherlands

This paper focuses on the attitude control and propellant slosh suppression of aeroelastic launch vehicles in a turbulent atmosphere. For a five-degree pitch-angle block command, the tracking performance of the selected Incremental Non-Linear Dynamic Inversion Sliding Mode Controller (INDI-SMC) shows excellent tracking performance. However, turbulence still inevitably leads to oscillatory behaviour in the swivel command. Various filter designs have been implemented to improve the smoothness of INDI-SMC. Using either a notch or band-pass filter in the sensor-feedback loops of pitch angle and pitch rate only marginally reduced the swivel oscillations, but did not solve the problem for the rigid-body control. For the flexible launcher with slosh dynamics, filtering of the sensor-feedback signals reduced the oscillations in swivel command, and elastic and slosh motion significantly, but could not completely remove them. The preliminary design of a rigid-body state observer has been included, and the results show that the INDI-SMC controller remains stable in the presence of engine dynamics, sloshing, flexible modes, input errors due to the use of rigid-body and slosh-state observers, while flying in a turbulent wind field.

I. Introduction

Launch systems, normally with long and slender bodies, may suffer from unwanted couplings between the rigid-body and structural modes, leading to stability and controllability issues when not properly dealt with. The high-frequency structural vibration modes can be excited by wind (gusts) and turbulence, and propagate to rigid-body degrees of freedom. Apart from these coupling effects, launchers with liquid-propellant propulsion systems also present the sloshing phenomenon, *i.e.,* (a part of) the fuel and oxidiser move in their corresponding tanks and induce perturbing accelerations. The sloshing effects can create a dynamic coupling with the rigid and/or flexible body that is not trivial to suppress. This is further complicated by the time-varying nature of the dynamic coupling, since the tank filling grades change significantly during the flight.

In literature, researchers have been devoted to the dynamic analyses and control design for flexible launchers with sloshing dynamics.[1–3] However, many methods assume perfect knowledge of the slosh motion by applying an equivalent mechanical model for control design. To design a realistic and effective control framework for launch systems, our earlier work has focused on the effect of aeroelasticity on launch-vehicle stability, controllability, and controller performance at a single point during the ascending flight,[4] as well as the additional effect of wind gust and turbulence during the trajectory from lift-off to burnout of the first stage, taking transient effects into account.[5] Moreover, to acquire the sloshing motions in real-time, we designed a sliding-mode observer to estimate the slosh states of the LOX and RP-1 tanks of the first stage.[6] Simulations show that the observer converges in a few seconds and is adequate for real-time sloshing suppression.

*Associate Professor, Section Astrodynamics and Space Missions, e.mooij@tudelft.nl, Associate Fellow AIAA.
†Assistant Professor, Section of Aerospace Structures and Computational Mechanics & Section of Control and Simulations, x.wang-6@tudelft.nl, AIAA Member.

One of the primary control objectives for launch systems is attitude tracking. However, due to the coupling effects, limit-cycle oscillations in both slosh states and swivel command can be present during an attitude tracking task, which cannot be suppressed by a simple PD controller.[6] To improve the control performance and robustness, an Incremental Non-linear Dynamic Inversion Sliding Mode Control (INDI-SMC) system was proposed in Ref. 7. INDI-SMC is a hybrid control framework derived for generic multi-input/multi-output non-linear uncertain systems. Its robustness against model uncertainties, sudden actuator faults, and structural damage has been demonstrated by Lyapunov-based analyses, numerical simulations, and real-world quadrotor flight tests.[8] As compared to the conventional model-based SMC designs in literature, the control model dependency and sliding-mode control/observer gains are simultaneously reduced in the INDI-SMC framework.

To the best of the authors' knowledge, Ref. 7 presents the first INDI-SMC design for *under-actuated* dynamic systems. By exploiting the null space, its sliding surface ensures the robustness of the controller against *unmatched* uncertainties. The closed-loop stability is also guaranteed in the Lyapunov sense. This method is applied to a command tracking problem of an aeroelastic launch vehicle with propellant slosh, and is compared with an Linear-quadratic Regulator (LQR) and a conventional SMC based on Feedback Linearisation (FL). In the nominal case, it has been demonstrated that conventional INDI control (without slosh-state feedback) is unable to suppress the slosh dynamics. On the contrary, LQR, FL-SMC, and the proposed INDI-SMC can suppress the sloshing dynamics while tracking the attitude commands. A sensitivity analysis also showed that INDI-SMC and FL-SMC can more effectively damp out the slosh motions than the LQR. Moreover, INDI-SMC leads to the smallest pitch-angle tracking error.[7]

The robustness of the controller to parametric uncertainties and un dynamics (aeroelastic modes and engine dynamics) have been verified by Monte-Carlo studies. It has been shown that the system using LQR has many outliers requiring significant control efforts. Moreover, INDI-SMC has better nominal performance, as well as smaller values for the maximum outliers than FL-SMC. The slosh energy using INDI-SMC is lower as well. It is noteworthy that INDI-SMC also requires less model information than FL-SMC. Various performance metrics have verified the superior robustness of INDI-SMC, including the integrated state deviation and the slosh motions.

Despite the promising robustness of INDI-SMC against parametric uncertainties, aeroelastic modes, and engine dynamics, its performance in a turbulent atmosphere has not been studied before. A turbulent atmosphere imposes both low-frequency and high-frequency excitations to the launch system, which induce motions and couplings in rigid-body, aeroelastic, sloshing, engine swivel degrees of freedom. To address this challenging task, in this paper we will study the effect of a turbulent wind field on the controller performance of a conventional, aeroelastic launch vehicle with sloshing. Both sensor and actuator-command filtering will be considered, and if this does not guarantee smooth control, the development of a rigid-body state observer will be considered.

As a reference, the two-stage PacAstro launcher for small payloads up to 225 kg has been selected for continuity of the research and the availability of launcher data[a]. The launcher is treated as a flexible beam with lumped masses to account for the subsystems and the fuel.[4–6] Modelling of the slosh motion will be done for oxidiser and fuel separately, with one tank each per stage of the selected two-stage launcher.

The layout of this paper is as follows. Section II will discuss the simulation model. Section III presents the incremental sliding mode controller. Next, in Sec. IV, the results of the study are shown. Section V gives and overview of the rigid-body state observer design, and the effect it has on the controller performance. Finally, Sec. VI concludes this paper with final remarks.

II. Flight-Dynamics Model

For stability and controllability studies of flexible launchers, it is common practise to focus on pitch-plane motion only, and then even considering a linearised system that represents the error dynamics. Following this approach, in previous work the state-space model for a flexible launcher with engine dynamics and coupled slosh dynamics has been derived.[4,10] In this section we will summarise this model, but refrain from the detailed mathematical expressions; the reader is referred to the earlier mentioned references.

[a]PacAstro was a US transportation service company, formed in 1990, to provide low-cost transportation of small satellites to Low Earth Orbit for approximately $5 million per launch using proven technology.[9] Unfortunately, the launcher never came to operation despite several engine tests and three launch contracts, due to the lack of development funding. The company ceased to be in 1997.

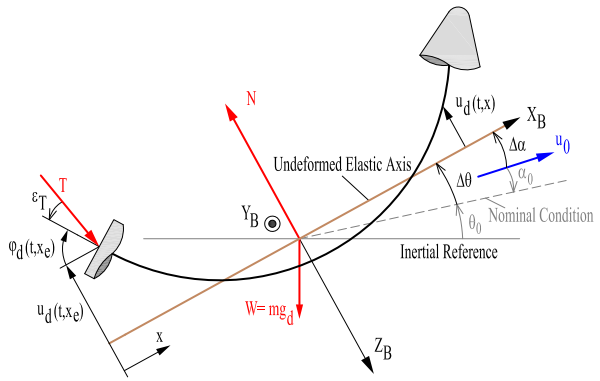

Figure 1. Flexible vehicle definitions

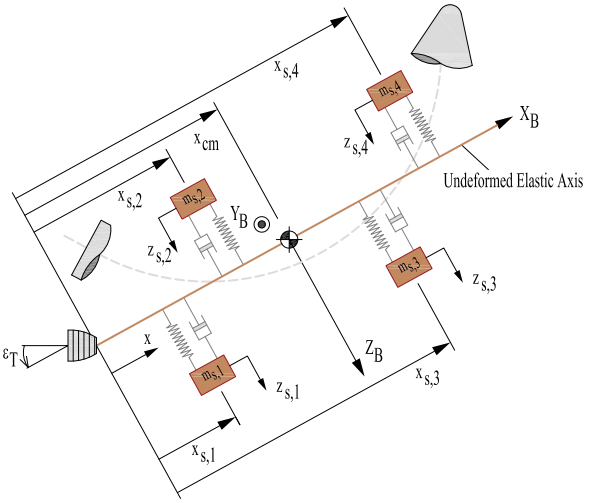

Figure 2. Slosh configuration of the flexible launcher

The flexible-launcher configuration that serves as the basis for the state-space model describing the error dynamics is shown in Fig. 1. Input to this error-dynamics model is a modal description as a function of current mass, the normal-load and pitch-moment distribution, and, of course, the flight conditions. The launcher is assumed to move with a steady-state velocity u_0. Its rotational states are the pitch angle, θ, and its derivative the pitch rate, q, and the angle of attack, α, that originates from the vertical velocity, and has been added to allow for adding wind effects as a perturbation in angle of attack. The local deformation is determined by the combination of thrust, T, gravity, mg_d, aerodynamic normal force, N, and aerodynamic pitch moment, M. The structural model is represented by a (discretised) flexible beam, and its modal shapes have been used to include the effects of elastic-line deformation in the aerodynamic coefficients. Finally, the engine is assumed to be 100% throttleable (albeit that in the current study the thrust is assumed constant), and its direction is given by the swivel angle, ε_T. The swivel is modelled as a third-order dynamics system, and its commanded input, $\varepsilon_{T,c}$, is the only control variable.

The liquid motion in the fuel and oxidiser tanks will introduce perturbing accelerations that affect the motion of the launcher. Besides the actual slosh dynamics, sloshing will introduce coupling effects with the rigid translational and rotational motion, as well as with the flexible-body dynamics. In Fig. 2 the configuration of the flexible launcher is shown, with two slosh masses, $m_{s,1}$ and $m_{s,2}$, for the RP-1 and LOX tanks of the first stage, and two for the second stage ($m_{s,3}$ and $m_{s,4}$). However, in this paper it is assumed that the second-stage tanks are completely filled and do not experience any sloshing. The slosh model for a cylindrical tank (partially) filled with fuel or oxidiser is based on a damped mass-spring system, developed by Abramson in the 1960s.[11,12]

In its general form, the system equation of the extended state-space model that is used for the plant (launcher) is given by

$$\mathbf{E}\dot{\mathbf{x}} = \mathbf{A}\mathbf{x} + \mathbf{B}\mathbf{u} \tag{1}$$

or

$$\dot{\mathbf{x}} = \mathbf{E}^{-1}\mathbf{A}\mathbf{x} + \mathbf{E}^{-1}\mathbf{B}\mathbf{u} = \mathbf{A}'\mathbf{x} + \mathbf{B}'\mathbf{u} \tag{2}$$

with the state and control vector given by $\mathbf{x}^{\mathrm{T}} = \left(\alpha\, \theta\, q\, \ddot{\varepsilon}_T\, \dot{\varepsilon}_T\, \varepsilon_T\, \dot{\eta}_1\, \eta_1 \ldots \dot{\eta}_{n_f}\, \eta_{n_f}\, \dot{z}_{s,1}\, z_{s,1} \ldots \dot{z}_{s,n_s}\, z_{s,n_s}\right)^{\mathrm{T}}$ and $\mathbf{u} = \varepsilon_{T,c}$ (the commanded swivel angle), respectively. The matrices $\mathbf{A}$ and $\mathbf{B}$ are the system and control matrix, respectively, whereas $\mathbf{E}$ is the (coupled) mass matrix.

Flying through a wind field will affect the angle of attack of the launcher, and will induce a perturbing pitch moment that is to be compensated for by the controller. The launcher used in this study is unstable for the design point under consideration ($C_{m_\alpha} > 0$), such that analysing the control-system performance in a perturbing wind environment is a necessity. Currently, we will restrict ourselves to wind turbulence,

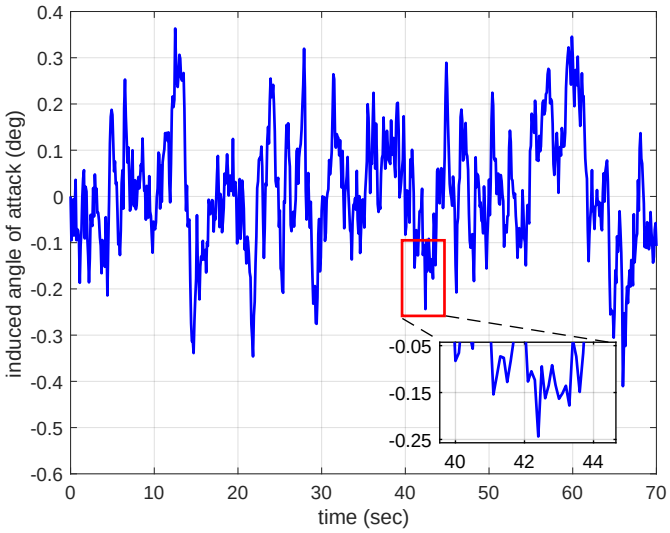

Figure 3. Induced angle of attack due to wind turbulence. From the insert a principal component with a frequency of about 2.5 Hz can be established.

which is modelled with Dryden spectral densities, as a white noise passing through a linear, rational filter.[13,14] Parameters used are a scale length at medium/high altitudes of $L_w = 1100$ m, a gust intensity of $\sigma_w = 1.73$ m/s, and a probability of exceedance of high-altitude intensity of 10^{-3} (moderate conditions). The model is evaluated as a function of altitude, h, and flight velocity, u_0, and will, in this case, produce a noisy wind component in the Z-direction, Δw. This can be converted to an equivalent angle-of-attack perturbation of $\Delta\alpha_t = \frac{\Delta w}{u_0}$. This perturbation is added as a forcing function to the state-space model, by creating a second input and extending the input matrix $\mathbf{B}$ with a copy of the first column of $\mathbf{A}$ (the one associated with α). As such, the system will respond to $\Delta\alpha_t$ as it would to α. In Fig. 3 the induced angle of attack due to wind turbulence is shown, for the point of maximum dynamic pressure ($h = 11{,}546$ m, $V = 508.1$ m/s, yielding a Mach number of $M = 1.90$). The induced angle of attack varies between $\pm 0.4°$. Despite the noisy pattern, one of the primary frequencies in the signal is one with a frequency of about 2.5 Hz. This frequency will show up later in the response results as well.

For the non-linear controller design to be discussed in the next section, we reformulate the above state-space system, and group some of the coupling effects and the engine dynamics. The error-dynamic model is now written in the following form:[10]

$$\ddot{\theta} - \frac{1}{I_{yy}} \sum_{j=1}^{2} m_{s,j} \ell_{s,j} \ddot{z}_{s,j} = f_q(t, \mathbf{x}, u) + \frac{T - D}{m I_{yy}} \sum_{j=1}^{n_s} m_{s,j} z_{s,j} \tag{3}$$

$$\ddot{z}_{s,j} + u_0 \dot{\alpha} - \ell_{s,j} \dot{q} + \sum_{i=1}^{n_f} \phi_i(x_{s,j}) \ddot{\eta}_i = \frac{T - D}{m} \theta - 2\zeta_{s,j} \omega_{s,j} \dot{z}_{s,j} - \omega_{s,j}^2 z_{s,j} \tag{4}$$

$$\dot{\alpha} + \frac{1}{m u_0} \sum_{j=1}^{2} m_{s,j} \ddot{z}_{s,j} = f_\alpha(t, \mathbf{x}, u, \alpha_{\text{dis}}) \tag{5}$$

$$\ddot{\eta}_i + \sum_{j=1}^{2} m_{s,j} \phi_i(x_{s,j}) \ddot{z}_{s,j} = f_\eta(t, \mathbf{x}, u) \tag{6}$$

In the above equation, θ and α represent the rigid-body states of the launch vehicle. The slosh dynamics is modelled as two mass-spring-damping systems (the primary mode for each tank in the first stage), where $m_{s,j}$ represents the slosh mass, $\omega_{s,j}$ and $\zeta_{s,j}$ are the eigenfrequency and damping ratio of the j^{th} slosh mode, and $z_{s,j}$ is the (position) state for the j^{th} slosh mode. T and D denote the total thrust and drag, respectively, whereas α_{dis} in f_α represents the angle of attack induced by external atmospheric disturbances

(include discrete gusts and turbulence). Finally, η_i is the generalised coordinate of the i^{th} flexible mode, and the coupling between flexible and slosh modes is enforced through the modal shape function, ϕ_i, at the axial slosh location $x_{s,j}$. For now, only two flexible modes with $\omega_{f,1} = 37.1$ rad/s and $\omega_{f,2} = 119.8$ rad/s will be considered.

III. Control Design

This paper aims at simultaneously achieving different control objectives using a single control input u. First of all, the controller should guarantee the stability of the closed-loop system. Then, the controller aims at driving θ towards its reference θ_c. The slosh dynamics should also be damped. Finally, the controller should be able to reject external disturbances and be robust to model uncertainties.

To begin with, $f_q(t, \mathbf{x}, u)$ in Eqs. (3)-(6) is explicitly written as

$$f_q(t,\mathbf{x},u) = \frac{C_{m_q}\bar{q}S_{\text{ref}}d_{\text{ref}}}{I_{yy}}q + \frac{C_{m_\alpha}\bar{q}S_{\text{ref}}d_{\text{ref}}}{I_{yy}}\alpha + \sum_{i=1}^{n_f} a_{q,\dot{\eta}_j}\dot{\eta}_j + \sum_{i=1}^{n_f} a_{q,\eta_j}\eta_j + \frac{L_eT}{I_{yy}}u \tag{7}$$

with $\bar{q}$ being the dynamic pressure, and $u = \varepsilon_{T,c}$ the commanded swivel angle, the only control input to the system.

Denote the acceleration along the elastic axis as $a_x = \frac{T-D}{m}$, using Eqs. (3) through (7), the dynamics of the launch vehicle are expressed as

$$\begin{bmatrix} 1 & -\frac{m_{s,1}\ell_{s,1}}{I_{yy}} & \dots & -\frac{m_{s,n_s}\ell_{s,n_s}}{I_{yy}} \\ -\ell_{s,1} & 1+\frac{m_{s,1}}{m} & \dots & \frac{m_{s,n_s}}{m} \\ \vdots & & \ddots & \\ -\ell_{s,n_s} & \frac{m_{s,1}}{m} & \dots & 1+\frac{m_{s,n_s}}{m} \end{bmatrix} \begin{pmatrix} \ddot{\theta} \\ \ddot{z}_{s,1} \\ \vdots \\ \ddot{z}_{s,n_s} \end{pmatrix} = \begin{bmatrix} \frac{C_{m_q}\bar{q}S_{\text{ref}}d_{\text{ref}}}{I_{yy}} & 0 & \dots & 0 \\ 0 & -2\zeta_{s,1}\omega_{s,1} & \dots & 0 \\ \vdots & & \ddots & \\ 0 & 0 & \dots & -2\zeta_{s,n_s}\omega_{s,n_s} \end{bmatrix} \begin{pmatrix} \dot{\theta} \\ \dot{z}_{s,1} \\ \vdots \\ \dot{z}_{s,n_s} \end{pmatrix}$$
$$+ \begin{bmatrix} 0 & \frac{a_x m_{s,1}}{I_{yy}} & \dots & \frac{a_x m_{s,n_s}}{I_{yy}} \\ a_x & -\omega_{s,1}^2 & \dots & 0 \\ \vdots & & \ddots & \\ a_x & 0 & \dots & -\omega_{s,n_s}^2 \end{bmatrix} \begin{pmatrix} \theta \\ z_{s,1} \\ \vdots \\ z_{s,n_s} \end{pmatrix} + \begin{pmatrix} \frac{L_eT}{I_{yy}} \\ 0 \\ \vdots \\ 0 \end{pmatrix} u + \begin{pmatrix} \frac{C_{m_\alpha}\bar{q}S_{\text{ref}}d_{\text{ref}}}{I_{yy}}\alpha + \sum_{i=1}^{n_f} a_{q,\dot{\eta}_j}\dot{\eta}_j + \sum_{i=1}^{n_f} a_{q,\eta_j}\eta_j \\ -u_0 f_\alpha - \sum_{i=1}^{n_f}\phi_i(x_{s,j})\ddot{\eta}_i \\ \vdots \\ -u_0 f_\alpha - \sum_{i=1}^{n_f}\phi_i(x_{s,j})\ddot{\eta}_i \end{pmatrix} \tag{8}$$

Equation (8) can be written in a condensed form as

$$\mathbf{M_s}\ddot{\mathbf{x}} = -\mathbf{C_s}\dot{\mathbf{x}} - \mathbf{K_s}\mathbf{x} + \mathbf{B}_s u + \mathbf{d}_s \tag{9}$$

The state vector is defined as $\mathbf{x} = [\theta, z_{s,1}, z_{s,2}, \dots, z_{s,n_s}]^{\mathrm{T}}$. Since $0 < m_{s,j} < m$ for all j, the mass matrix $\mathbf{M}_s$ in Eq. (9) is always invertible. The non-zero off-diagonal elements of $\mathbf{M}_s$ reflect the inertial couplings between the pitch and slosh dynamics. From Eq. (9), the launch-vehicle pitch dynamics is written as

$$\ddot{\theta} = f_\theta(\dot{\theta}, \theta, \dot{z}_{s,j}, z_{s,j}) + Gu + d_\theta \tag{10}$$

in which f_θ represents the first row of $\mathbf{M_s}^{-1}(-\mathbf{C_s}\dot{\mathbf{x}} - \mathbf{K_s}\mathbf{x})$, while d_θ represents the first row of $\mathbf{M_s}^{-1}\mathbf{d}_s$ in Eq. (9). The control effectiveness G equals the first row of $\mathbf{M_s}^{-1}\mathbf{B}_s$.

Assumption 1 *G is non-singular for all t.*

A. Partial Feedback Linearisation

The dynamic system given in Eq. (8) contains coupled rigid-body pitch and slosh dynamics. However, there is only one single control input to the system. Therefore, the control problem of simultaneously stabilising θ and slosh states becomes an under-actuated problem. Since rigid-body motion control has higher priority, the controlled output variable is selected as $y = \theta$. The sensor-based Incremental Non-linear Dynamic Inversion (INDI) was proposed in Ref. 7. Recently, INDI was generalised to generic multi-input/multi-output non-linear systems.[15] The partial input-output feedback linearisation can also be achieved by INDI. Denote the

sampling interval as Δt. Taking the first-order Taylor series expansion of Eq. (10) around the condition at $t-\Delta t$ (denoted by the subscript 0) results in

$$\begin{aligned}\ddot{\theta} &= f_\theta(\dot{\theta},\theta,\dot{z}_{s,j},z_{s,j})+Gu+d_\theta \\ &= \ddot{\theta}_0+\left.\frac{\partial f_\theta}{\partial\dot{\theta}}\right|_0\Delta\dot{\theta}+\left.\frac{\partial f_\theta}{\partial\theta}\right|_0\Delta\theta+\sum_{j=1}^{n_s}\left.\frac{\partial f_\theta}{\partial\dot{z}_{s,j}}\right|_0\Delta\dot{z}_{s,j}+\sum_{j=1}^{n_s}\left.\frac{\partial f_\theta}{\partial z_{s,j}}\right|_0\Delta z_{s,j}+G_0\Delta u+\Delta d_\theta+R_1\end{aligned} \tag{11}$$

where $\Delta(\cdot)$ represents the variations of $(\cdot)$ in one sampling interval Δt. R_1 in Eq. (11) is the expansion remainder. The incremental control is designed as

$$\Delta u=(\nu-\ddot{\theta}_0)/\hat{G}_0 \tag{12}$$

The actual actuator control command equals $u=u_0+\Delta u$, where u_0 is the control input at $t-\Delta t$. Substituting Eq. (12) into Eq. (11) leads to

$$\begin{aligned}\ddot{\theta} &= \nu+(G_0-\hat{G}_0)\Delta u+\Delta d_\theta+\left(\left.\frac{\partial f_\theta}{\partial\dot{\theta}}\right|_0\Delta\dot{\theta}+\left.\frac{\partial f_\theta}{\partial\theta}\right|_0\Delta\theta+\sum_{j=1}^{n_s}\left.\frac{\partial f_\theta}{\partial\dot{z}_{s,j}}\right|_0\Delta\dot{z}_{s,j}+\sum_{j=1}^{n_s}\left.\frac{\partial f_\theta}{\partial z_{s,j}}\right|_0\Delta z_{s,j}+R_1\right) \\ &\triangleq \nu+(G_0-\hat{G}_0)\Delta u+\Delta d_\theta+\delta(\mathbf{x},\dot{\mathbf{x}},t)\triangleq\nu+\varepsilon_{\text{indi}}\end{aligned} \tag{13}$$

In Eq. (13), $\delta(\mathbf{x},\dot{\mathbf{x}},t)$ represents the closed-loop value of the state variations and expansion remainders. $\varepsilon_{\text{indi}}$ is the lumped uncertainty term under INDI control.

Assumption 2 *The lumped variation term $\delta(\mathbf{x},\dot{\mathbf{x}},t)$ in Eq. (13) satisfies $|\delta(\mathbf{x},\dot{\mathbf{x}},t)|\le\bar{\delta}$.*

In view of Eq. (8), $\mathbf{x}$ is twice continuously differentiable. Therefore, $\lim_{\Delta t\to 0}\|\Delta\mathbf{x}\|_2=0$ and $\lim_{\Delta t\to 0}\|\Delta\dot{\mathbf{x}}\|_2=0$. If the first-order and second-order partial derivatives of f_θ with respect to $\mathbf{x}$ and $\dot{\mathbf{x}}$ are bounded, then it can be seen from Eq. (13) that the absolute value of $\delta(\mathbf{x},\dot{\mathbf{x}},t)$ approaches zero as Δt decreases. Therefore, this assumption can be met by the selection of a sufficiently small sampling interval.

Proposition 1 (Ref. 7) *Under Assumptions 1 and 2, if $|1-G/\hat{G}|\le\bar{b}<1$ for all t, then for sufficiently small sampling interval Δt, the residual error ε_{indi} in Eq. (13) is ultimately bounded.*

B. Virtual Control Design

To simultaneously achieve rigid-body state tracking and slosh suppression, the incremental sliding mode control (INDI-SMC) will be used. Define the new state vector as $\mathbf{X}=[\dot{\theta},\theta,\dot{z}_{s,1},z_{s,1},\ldots,\dot{z}_{s,n_s},z_{s,n_s}]^{\mathrm{T}}$, and define its reference vector as $\mathbf{X}_{\text{ref}}=[\dot{\theta}_{\text{ref}},\theta_{\text{ref}},0,0,\ldots,0,0]^{\mathrm{T}}$, then the dynamics of the tracking error $\mathbf{e}=\mathbf{X}-\mathbf{X}_{\text{ref}}$ are written as[7]

$$\dot{\mathbf{e}}=\mathbf{A}\mathbf{X}+\mathbf{B}\nu+\mathbf{d}-\dot{\mathbf{X}}_{\text{ref}}=\hat{\mathbf{A}}\mathbf{X}+\hat{\mathbf{B}}\nu+(\mathbf{A}-\hat{\mathbf{A}})\mathbf{X}+(\mathbf{B}-\hat{\mathbf{B}})\nu+\mathbf{d}-\dot{\mathbf{X}}_{\text{ref}} \tag{14}$$

where only the estimated $\hat{\mathbf{A}}$ and $\hat{\mathbf{B}}$ are available for control-system design. The model uncertainties and external disturbances can be classified into matched and unmatched uncertainties. Because $\varepsilon_{\text{ndi/indi}}$ enters the state equation at the same point as the virtual control input ν, it is a matched uncertainty term. Although sliding mode control has inherent robustness to matched uncertainties, the sliding surface should be carefully designed to ensure the robustness to unmatched uncertainties, which in this case, are the uncertain system elements $a_{i,j},\ i=1,...,n_s,\ j=1,...,2n_s+2$, $b_1,...,b_{n_s}$, and $d_1,...,d_{n_s}$.

Design the sliding surface as $s=\mathbf{C}^{\mathrm{T}}\mathbf{e}=0$, where $\mathbf{C}\in\mathbb{R}^{(2n_s+2)\times 1}$. This vector $\mathbf{C}$ is designed such that the unmatched uncertainties belong to the *null space* of $\mathbf{C}^{\mathrm{T}}$, while $\mathbf{C}^{\mathrm{T}}\hat{\mathbf{B}}$ should still be invertible. In this paper, $\mathbf{C}$ is designed as

$$\mathbf{C}=[1,c_\theta,0,c_1,\ldots,0,c_{n_s}]^{\mathrm{T}} \tag{15}$$

The following equations can be verified

$$\mathbf{C}^{\mathrm{T}}(\mathbf{A}-\hat{\mathbf{A}})=\mathbf{0},\quad \mathbf{C}^{\mathrm{T}}(\mathbf{B}-\hat{\mathbf{B}})=0,\quad \mathbf{C}^{\mathrm{T}}\hat{\mathbf{B}}=1,\quad \mathbf{C}^{\mathrm{T}}\mathbf{d}=\varepsilon_{\text{ndi/indi}} \tag{16}$$

Lemma 1 (Ref. 17) *If a Lyapunov function V satisfies $\dot{V} + \alpha V + \beta V^{\gamma} \leq 0,\ \alpha, \beta > 0,\ 0 < \gamma < 1$, then $V = 0$ will be reached in finite time $T \leq \frac{1}{\alpha(1-\gamma)} \ln \frac{\alpha V^{1-\gamma}(t_0)+\beta}{\beta}$.*

Theorem 1 (Ref. 7) *For the system modelled by Eq. (14) with sliding surface $s = \mathbf{C}^{\mathrm{T}}\mathbf{e} = 0$, where $\mathbf{C}$ is given by Eq. (15), design $\nu = -k_1 s - k_2 |s|^{\rho} sign(s) - \mathbf{C}^{\mathrm{T}}\hat{\mathbf{A}}\mathbf{X} + \mathbf{C}^{\mathrm{T}}\dot{\mathbf{X}}_{ref}$, $k_1 > 0, k_2 > \eta > 0, 0 < \rho < 1$, then*

1. *In the absence of the perturbation term $\varepsilon_{ndi/indi}$, $s = 0$ is reached in finite time.*
2. *If the perturbation term $\varepsilon_{ndi/indi}$ is bounded, then the system trajectories will converge to the neighbourhood of $s = 0$ as $s \leq \bar{s}_{ndi/indi} = (|\varepsilon_{ndi/indi}|/(k_2 - \eta))^{\frac{1}{\rho}}$ in finite time.*

It is noteworthy that the sliding surface designed in this paper guarantees that all the unmatched uncertainties belong to the null space of $\mathbf{C}^{\mathrm{T}}$, and the resulting dynamics is only perturbed by $\varepsilon_{\mathrm{ndi/indi}}$, which lies in the input channel of ν.

On the sliding surface, the equivalent virtual control is $\nu_{\mathrm{eq}} = -\mathbf{C}^{\mathrm{T}}\hat{\mathbf{A}}\mathbf{X} + \mathbf{C}^{\mathrm{T}}\dot{\mathbf{X}}_{\mathrm{ref}}$, which is calculated by substituting $s = 0$ into the ν given in Theorem 1. Therefore, the equivalent closed-loop dynamics is

$$\dot{\mathbf{e}} = \mathbf{A}\mathbf{X} + \mathbf{B}\nu + \mathbf{d} - \dot{\mathbf{X}}_{\mathrm{ref}} = \mathbf{A}\mathbf{X} + \mathbf{B}(-\mathbf{C}^{\mathrm{T}}\hat{\mathbf{A}}\mathbf{X} + \mathbf{C}^{\mathrm{T}}\dot{\mathbf{X}}_{\mathrm{ref}}) + \mathbf{d} - \dot{\mathbf{X}}_{\mathrm{ref}} \tag{17}$$

Since $\mathbf{C}^{\mathrm{T}}(\mathbf{A} - \hat{\mathbf{A}}) = \mathbf{0}$ (Eq. (16)), then

$$\dot{\mathbf{e}} = (\mathbf{I} - \mathbf{B}\mathbf{C}^{\mathrm{T}})\mathbf{A}\mathbf{X} - (\mathbf{I} - \mathbf{B}\mathbf{C}^{\mathrm{T}})\dot{\mathbf{X}}_{\mathrm{ref}} + \mathbf{d} \tag{18}$$

Consider θ_{ref} as a piecewise linear signal such that $\ddot{\theta}_{\mathrm{ref}} = 0$. Because $\mathbf{X}_{\mathrm{ref}} = [\dot{\theta}_{\mathrm{ref}}, \theta_{\mathrm{ref}}, 0, 0, \ldots, 0, 0]^{\mathrm{T}}$. It can be seen that $\dot{\mathbf{X}}_{\mathrm{ref}} = \mathbf{A}\mathbf{X}_{\mathrm{ref}}$. Substituting this equation into Eq. (18) yields

$$\dot{\mathbf{e}} = (\mathbf{I} - \mathbf{B}\mathbf{C}^{\mathrm{T}})\mathbf{A}\mathbf{e} + \mathbf{d} \triangleq \mathbf{A}_{\mathrm{e}}\mathbf{e} + \mathbf{d} \tag{19}$$

Although $\mathbf{A}_{\mathrm{e}} \in \mathbb{R}^{(2n_s+2)\times(2n_s+2)}$, it can be examined that the rank of $\mathbf{A}_e$ equals $2n_s + 1$. This shows that on the sliding surface, the closed-loop system behaves as its reduced dynamics. To analyse the stability of the reduced-order dynamics, select $\mathbf{e}_r = \mathbf{T}\mathbf{e}$, where $\mathbf{T} \in \mathbb{R}^{(2n_s+1)\times(2n_s+2)}$, and ensure the rank of $\mathbf{T}$ equals $2n_s + 1$. Without loss of generality, select $\mathbf{e}_r = [e_\theta, \dot{z}_{s,1}, z_{s,1}, \ldots, \dot{z}_{s,n_s}, z_{s,n_s}]$, then Eq. (19) is rewritten as

$$\begin{pmatrix} \dot{e}_{\dot{\theta}} \\ \dot{\mathbf{e}}_r \end{pmatrix} = \begin{bmatrix} A_{11} & \mathbf{A}_{12} \\ \mathbf{A}_{21} & \mathbf{A}_{22} \end{bmatrix} \begin{pmatrix} e_{\dot{\theta}} \\ \mathbf{e}_r \end{pmatrix} + \begin{pmatrix} \varepsilon_{\mathrm{ndi/indi}} \\ \mathbf{d}_r \end{pmatrix} \tag{20}$$

On the sliding surface, $s = \mathbf{C}^{\mathrm{T}}\mathbf{e} = [1, c_\theta, 0, c_1, \ldots, 0, c_{n_s}]\mathbf{e} = 0$. Therefore, $\dot{e}_{\dot{\theta}} = -[c_\theta, 0, c_1, \ldots, 0, c_{n_s}]\mathbf{e}_r$. Substituting this relationship into Eq. (20), the reduced-order dynamics is

$$\dot{\mathbf{e}}_r = \mathbf{A}_{22}\mathbf{e}_r - \mathbf{A}_{21}[c_\theta, 0, c_1, \ldots, 0, c_{n_s}]\mathbf{e}_r + \mathbf{d}_r \triangleq \mathbf{A}_{rr}\mathbf{e}_r + \mathbf{d}_r \tag{21}$$

Recall Eq. (8), $\mathbf{d}_r$ contains the aerodynamic force f_α and the elastic perturbations. A part of these perturbations vanishes at the origin ($\alpha = q = z_{s,j} = \eta_i = 0$), while the remaining terms caused by the disturbing angle of attack α_{dis} are non-vanishing perturbations, thus the following assumption is made:

Assumption 3 *In Eq. (21) $\|\mathbf{d}_r\|_2 \leq \gamma_d \|\mathbf{e}_r\|_2 + \varepsilon_d$.*

Theorem 2 (Ref. 7) *Under Assumption 3, if $\mathbf{C}$ in Eq. (15) is designed such that $\mathbf{A}_{rr}$ in Eq. (21) is Hurwitz, and if $\gamma_d < \frac{1}{2\|\mathbf{P}\|_2}$, where $\mathbf{P} = \mathbf{P}^{\mathrm{T}} > 0$ is the solution of the Lyapunov function $\mathbf{P}\mathbf{A}_{rr} + \mathbf{A}_{rr}^{\mathrm{T}}\mathbf{P} = -\mathbf{I}$, then on the sliding surface $s = \mathbf{C}^{\mathrm{T}}\mathbf{e} = 0$, the tracking error vector $\mathbf{e}$ in Eq. (14) is ultimately bounded.*

A block diagram for INDI-SMC is shown in Fig. 4.

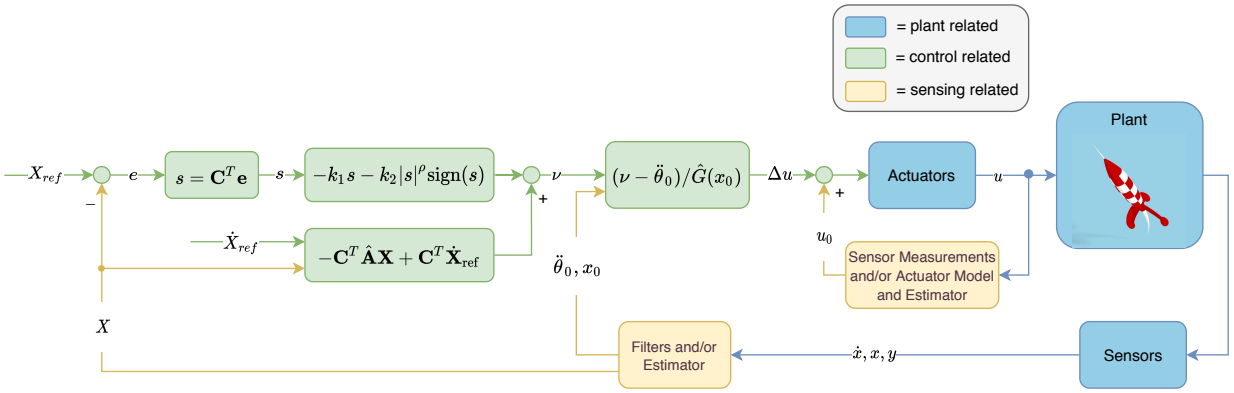

Figure 4. Block diagram for INDI-SMC.

IV. Results and Discussions

The analysis of controller performance will be done in several steps, using previously designed controllers first to establish a benchmark[6,7] for the rigid-body configuration flying through a turbulent wind field. The first controller is a state-feedback controller with feedback signals on pitch angle, pitch rate and the slosh states on position and velocity (one mode per tank),[6] effectively making this a PD controller[b]. The second controller is the earlier discussed INDI-SMC controller.[7]

For the actual study, the configuration of the plant is that of a flexible-body representation of the launcher, with a LOX and RP-1 tank in the first stage that can exhibit sloshing. The point of interest is that of maximum dynamic pressure, *i.e.,* at $t = 63.5$ s into the launch. Information about the launch trajectory, and the details about the state variables can be found in Ref. 4.

For both controllers, initially perfect state knowledge on both the rigid body and the two slosh modes is assumed. The slosh observer developed in Ref. 6 has shown to be working well to provide slosh-state knowledge. In Sec. V also a (rigid-)state observer will be included, *i.e.,* one that works well in the presence of turbulence and other uncertainties, and its interaction with the slosh observer. It is stressed that the angle of attack is not fed back to the controller. Any turbulence-induced angle of attack is therefore treated as a perturbation that will excite the rigid-body motion through the (unstable) aerodynamics acting on the system.

To minimise slosh excitation due to discrete command changes, a first-order pre-filter that smoothens the command is included in the pitch-angle channel. The transfer function of this command shaper is given by

$$H_c(s) = \frac{1}{\tau s + 1} \tag{22}$$

with time constant $\tau = 1.25$ s.

From earlier results, we had found that some form of actuator-dynamics estimation is required to avoid excitation of this dynamics by abrupt changes in actuator commands.[7] The simple solution applied consists of including a low-pass filter in the feedback loops of $\varepsilon_{T,0}$, *i.e.,* the engine state at the previous sample, and $\dot{q}$, the angular acceleration. Even when no actuator dynamics is simulated, these low-pass filters help to smoothen the transient response. The first-order low-pass filter (with a bandwidth equal to $\omega_a = 30$ rad/s) is given by

$$H_a(s) = \frac{\omega_a}{s + \omega_a} \tag{23}$$

The manoeuvre that will be executed is a step command in pitch angle, *i.e.,* $\theta_c = 5°$. In succession, we will discuss the rigid-body results in Sec. IV.A, starting with the benchmark and then trying to find

[b]The controller is a Linear Quadratic Regulator, designed for a relatively smooth response with a maximum state deviation of $\Delta\theta = 1°$, $\Delta q = 5°/\text{s}$, $\Delta\dot{z}_s = 30$ m/s and $\Delta z_s = 40$ m. The latter two large deviations have been selected to avoid a strong controller response due to more violent slosh motion. With a maximum swivel angle of $\Delta\varepsilon_T = 6°$, this gives the gains $\mathbf{K_{lqr}} = \begin{pmatrix} 6.07 & 1.37 & -0.0045 & -0.0154 & -0.0027 & -0.0148 \end{pmatrix}$, associated with states θ, q, $\dot{z}_{s,1}$, $z_{s,1}$, $\dot{z}_{s,2}$ and $z_{s,2}$.

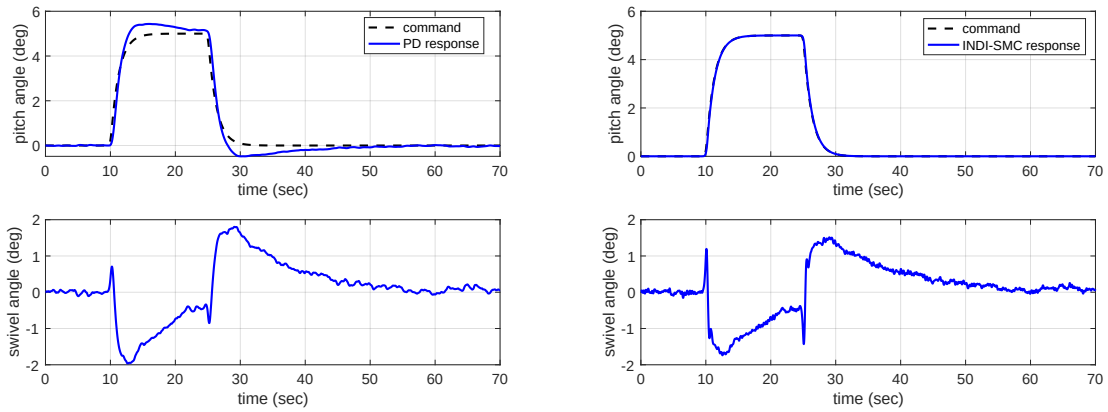

(a) PD (b) INDI-SMC

Figure 5. Benchmark performance for rigid launcher: $\theta_c = 5°$, turbulent wind field.

Table 1. Sensor-filter constants and parameters

	c_2	c_1	c_0	ζ_{co}	ω_{co}
Low-pass filter	0.0	0.0	1.0	1.00	to be selected
Notch filter	1.0	0.0	1.0	0.60	to be selected
Band-pass filter	0.0	2 ζ_{co}	0.0	0.16	to be selected

solutions to reduce the influence of turbulence. Then, in Sec. IV.B flexibility and sloshing are included in the model. Finally, in Sec. IV.C a third-order model representing the engine dynamics is added, such that the effect of a more realistic actuator model can be studied as well.

A. Rigid-Body Configuration

The first result for the rigid-body simulation is that of a commanded step in pitch angle of $\theta_c = 5°$ at $t = 10$ s. After $\Delta t = 15$ s, the command is released and the system should go back to equilibrium. In Fig. 5 the result is shown for both the PD controller and the INDI-SMC. Both controllers seem to be handling the turbulence quite well, although the swivel command is not smooth, and exhibits the random pattern induced by the perturbing angle of attack.

From inspecting the results, it is clear that the PD-controller performance is not optimal, showing an overshoot of about 0.5° (= 10%). On the other hand, the random oscillation in the swivel command is less than that of the INDI-SMC. Both controllers operate with the same frequency ($f_{control} = 100$ Hz), but the gains in each controller are different. The INDI-SMC has larger gains, which results on one hand in a much tighter command tracking, but on the other hand in a stronger noise amplification. Without loosing out on command tracking, the task at hand will be to find a solution to remove the noise. As the INDI-SMC has proven to be an otherwise very robust controller,[7] this will be the focus of the remaining research.

As a first step we will restrict ourselves to the category of filters, which we used in previous research to filter out vibrations in the sensor feedback due to the flexible motion:[18] a low-pass filter, a notch filter, and a band-pass filter. The generalised transfer function of the (second-order) filter is

$$H_b(s) = \frac{c_2 s^2 + c_1 \omega_{co} s + c_0 \omega_{co}^2}{s^2 + 2\zeta_{co}\omega_{co} s + \omega_{co}^2} \tag{24}$$

where c_0, c_1, and c_2 are constants, and ζ_{co} and ω_{co} are the damping and cut-off frequency, respectively. Different values for the constants and parameters will determine the type of filter. In Table 1 the relevant data are listed. The selection of cut-off frequency will be analysed through a Monte-Carlo analysis.

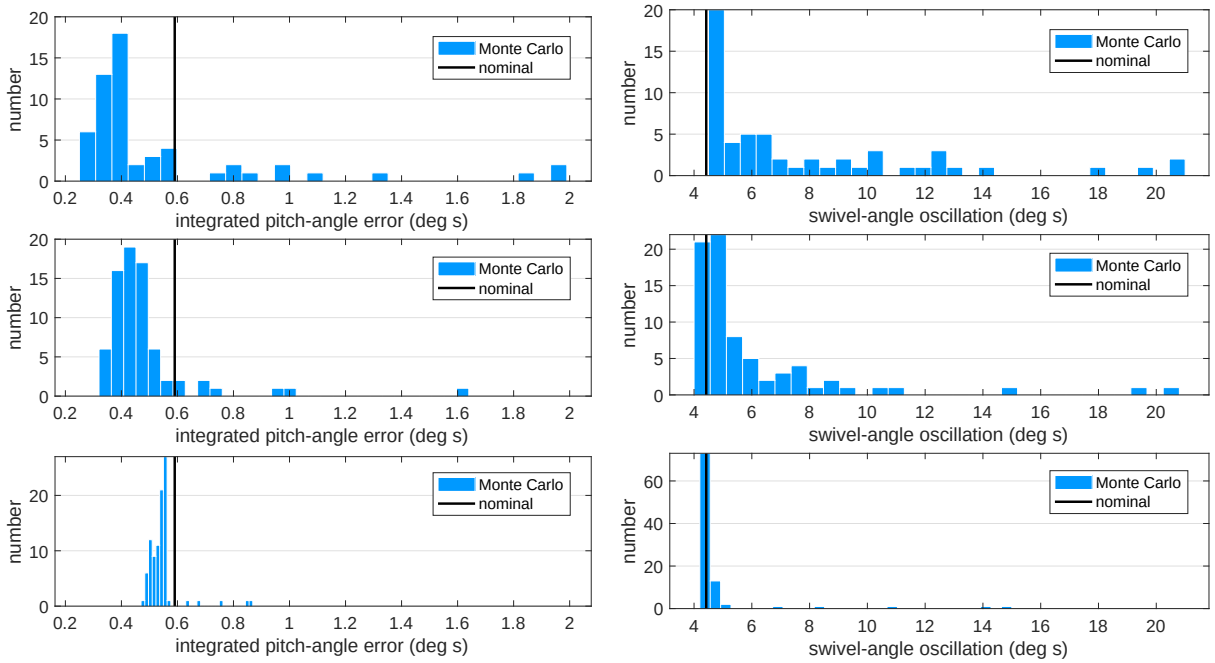

(a) Integrated state error

(b) Swivel oscillation

Figure 6. Transient response for flexible launcher with sloshing: $\theta_c = 5°$, turbulent wind field. Top to bottom: low-pass, notch and band-pass filter in both feedback loops.

For the analysis, we will evaluate the performance indices defined and explained in Appendix A: the integrated state deviation, $\sum_{\theta_{err}}$, integrated control effort, $\sum_{\varepsilon_T}$, and the corresponding oscillation indices, F_θ and F_{ε_T}. For both feedback of θ and q (representing "sensor measurements") one of the available filters will be inserted, where the cut-off frequency is varied between 20 and 100 rad/s. The following five configurations are analysed:

1. Low-pass filter for both θ and q,
2. Low-pass filter for θ and a notch filter for q,
3. Notch filter for θ and a low-pass filter for q,
4. Notch filter for both θ and q, and
5. A band-pass filter for both θ and q.

A total of N= 100 simulations will be run, while varying $\omega^2_{co,\theta}$ and $\omega^2_{co,q}$. This number of simulations was chosen due to the non-linear relationship between the filter parameters and the performance indices.

In Fig. 6, a subset of the results has been plotted, *i.e.,* the low-pass, notch and band-pass filter in both feedback loops, whereas the runs with a large oscillation ($> 50°$ s) have been removed for ease of visualisation. The low pass filter does not reduce the oscillations at all, and of the other two the notch filter is performing slightly better, both in terms of integrated pitch-angle error and swivel-angle oscillation.

Of course, a simultaneous reduction in both indices is required for a good performance, so to check that the results for the notch and band-pass filter are plotted in a scatter plot as well (Fig. 7). It confirms that the combined performance of the notch filter is marginally better, although the band-pass filter has the smaller oscillation values, albeit with minimum difference. But, as far as performance improvement goes, neither filter is able to remove the oscillations due to turbulence.

A similar analysis was done with either a low-pass, notch or band-pass filter in the swivel-command loop. However, any cut-off frequency selected between 20 and 100 rad/s made the performance worse, with the the higher frequency approaching the situation without filter. This led to believe that filtering the signal

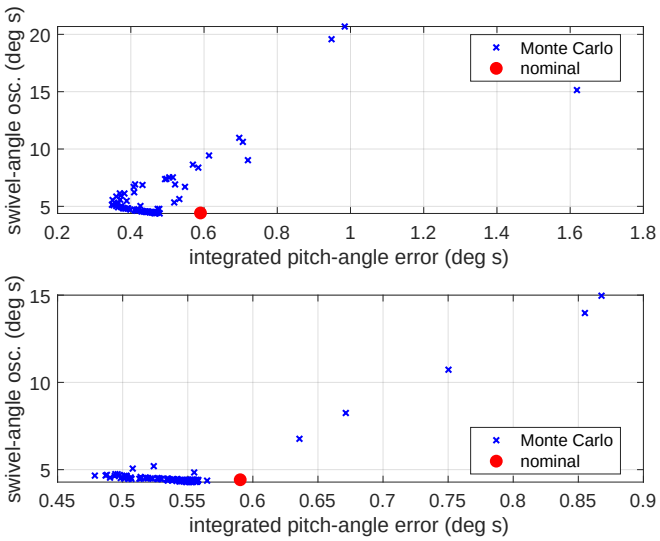

Figure 7. Swivel-angle oscillation versus integrated pitch-angle error, for the notch filter (top) and band-pass filter (bottom).

with at least these three filters would not solve the problem. Also the combination with the earlier discussed sensor filters would not yield the same performance as those without the actuator filter.

B. Flexible Launcher with Sloshing

The effect of turbulence on the flexible launcher with sloshing effects included is a lot more severe compared to the rigid-launcher response. Figure 8(a) shows the response to the same step function as before. The initially diverging oscillations of the swivel seem to have reached an oscillation with constant amplitude of $\pm 1.7°$. This is, of course, not good for the hardware involved. Also, even though the pitch angle is only marginally "vibrating", inspecting the flexible modes and the slosh motion, shows significant activity.

By including band-pass filters[c] in the sensor feedback loops for both θ and q, and after limited variation selecting $\omega_{co,\theta} = \omega_{co,q}$ shows a significant improvement (Fig. 8(b)), not only significantly reducing the amplitude, but also suppressing the divergent behaviour. It goes without saying that the smaller swivel oscillation will have a positive effect on the elastic vibrations and slosh motion.

The remaining oscillations in swivel angle has the already mentioned frequency of about 2.5 Hz, see the insert in the figure. We could see a similar frequency in the induced angle of attack due to the turbulent wind field (Fig. 3). Why this frequency remains so visibly present in the response remains to be studied.

To try and reduce the swivel oscillation even more, we will search for more optimal values for $\omega_{co,\theta}$ and $\omega_{co,q}$. Doing this with a limited Monte Carlo analysis and selecting the filter-frequency combination that gives the lowest swivel oscillation index, yields $\omega_{co,\theta} = 94.7$ rad/s and $\omega_{co,q} = 30.4$ rad/s. The resulting response plots are given in Figs. 9 and 10.

The rigid-body response in Fig. 9(a) shows that only a small oscillation is left in the swivel angle, slightly larger than the one for the actual rigid launcher (Fig. 5). The minor amplification is due to the coupling with the flexible mode and the slosh dynamics. Despite being more irregular, the 2.5 Hz frequency can still be found in the signal. It is even clearer by looking at the flexible mode (Fig. 9(b)), where a very distinct 2.5 Hz signal can be seen.

It is also obvious that with stronger control actions, *i.e.,* when the step commands are executed, both the flexible mode and the slosh dynamics are excited to large values. This, in turn, will have a cross coupling with the swivel command, seen as some "spiky" oscillations. The slosh masses clash with the tank wall, as seen in the constrained positions in Fig. 10.

[c]Band-pass filters have been selected over notch filters, as the phase lag induced by band-pass filters was found to be smaller in a previous study.[18] As the filtering performance of either filter is almost the same, the band-pass filter would be the preferred choice.

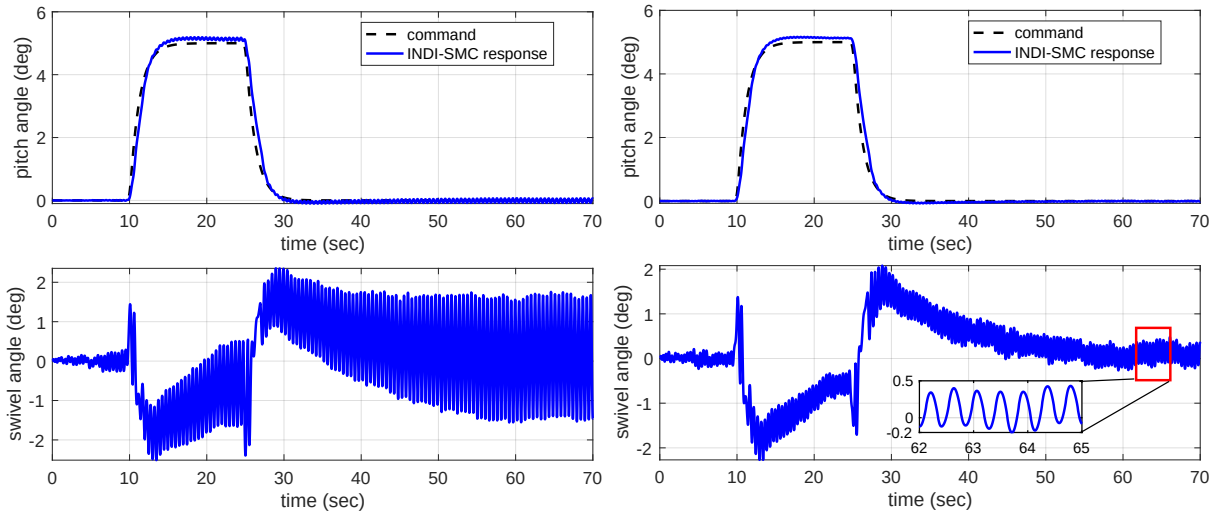

(a) Unfiltered (b) Filtered

Figure 8. Transient response for flexible launcher with sloshing: $\theta_c = 5°$, turbulent wind field.

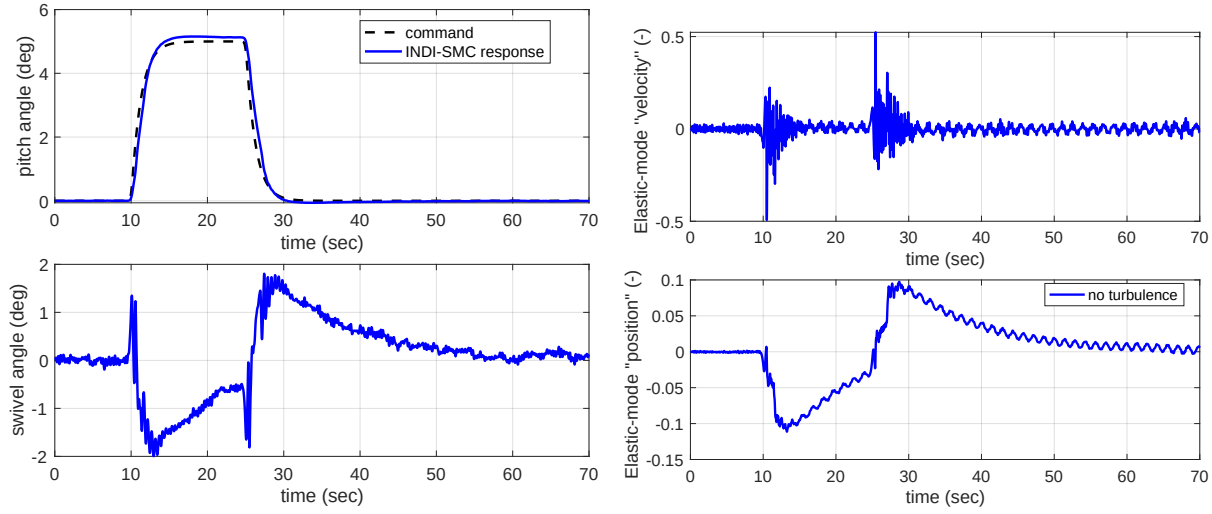

(a) Rigid body (b) Filtered

Figure 9. Transient response for flexible launcher with sloshing and optimal feedback-signal filtering: $\theta_c = 5°$, turbulent wind field.

Despite these strong dynamics effects, the INDI-SMC handles itself well. But once more, the conclusion is clear that the (simple) sensor filtering applied here is not sufficient to counter the perturbing effect of wind turbulence. In Sec. V, a rigid-body state estimator/observer will be developed that will smoothen the sensor feedback.

C. Flexible Launcher with Sloshing and Engine Dynamics

The simulations so far were restricted to the flexible launcher with ideal actuator dynamics, albeit that a filter was included in the feedback-control loop of the INDI-SMC to avoid discrete changes in actuator commands, see Eq. (23). However, in earlier research the engine was assumed to be an electro-hydraulic servo system, approximated by a third-order system:[4]

$$\left(s^3 + 2\zeta_e\omega_e s^2 + \omega_e^2 s + K_e\omega_e^2\right)\varepsilon_T = K_e\omega_e^2\varepsilon_{T,c} \tag{25}$$

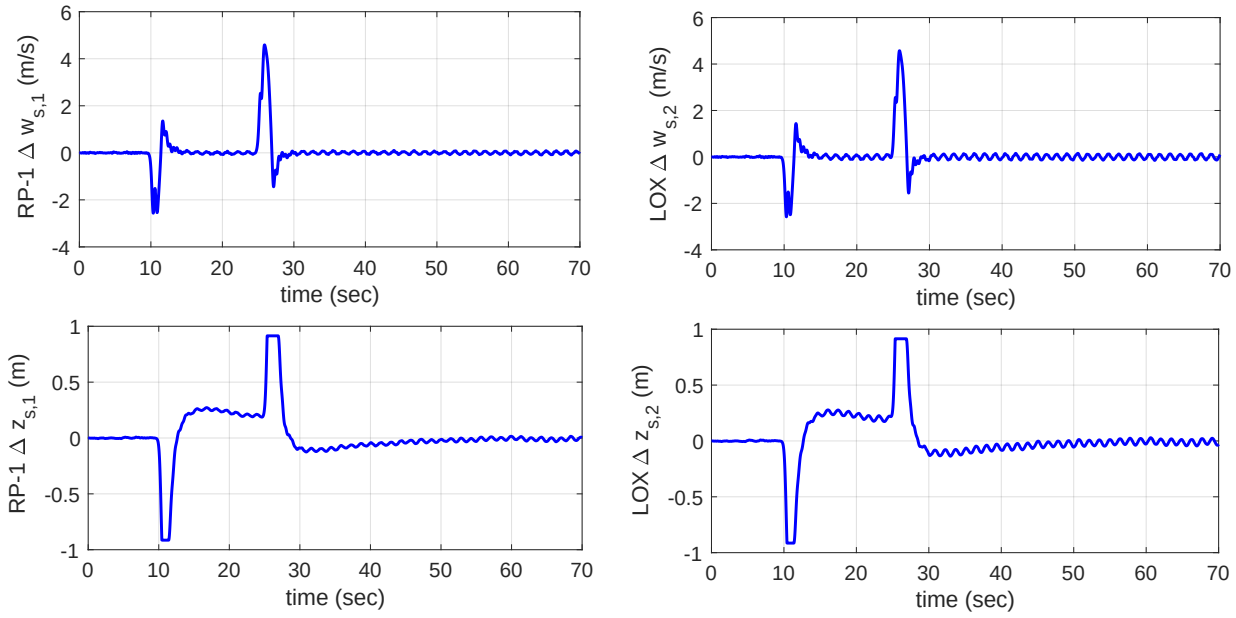

Figure 10. Transient response for flexible launcher with sloshing and optimal feedback-signal filtering: $\theta_c = 5°$, turbulent wind field.

with the amplification factor $K_e = 15$, the natural frequency $\omega_e = 50$ rad/s, and the damping $\zeta_e = 0.7$. Input to the model is the commanded swivel angle, $\varepsilon_{T,c}$, whereas the output is the actual angle, together with the swivel acceleration and velocity. Including this model, however, shows that the response becomes highly oscillatory even without the turbulent wind field, yet remains stable.

For the continuation of the research, this is an issue to be solved. Two aspects appeared to be important. In the first place, the actuator filter Eq. (23) interfered with the engine dynamics, and was therefore removed. This also applied to the sensor filter, studied in the previous section. In the second place, the step command with command-shaping function Eq. (22) had to be adjusted. Despite the fact that this shaping function smoothens the command when reaching the setpoint, it still has a discrete change in gradient when the command is given. The engine dynamics is excited in a sort of bang-bang mode because of this, resulting in strong variations in angular pitch rate and acceleration. These large-amplitude oscillations are very hard to handle by any controller.

The smooth step function that is implemented is given by the sigmoid function, chosen because of its differentiable property up to any order:

$$f_r(t) = \frac{1}{1 + e^{-at}} \tag{26}$$

The difference with the command-shaping filter is shown in Fig. 11.

The last change that was studied for this most complete (and dynamic) model, is whether the current controller parameters are still the best choice. Variation of the design parameters as indicated in Fig. 4, *i.e.,* $\mathbf{C}$, k_1, k_2, ρ (according to theory, limited to values betwee 0 and 1), and the control effectiveness $\hat{G}$ in a simple Monte-Carlo variation, led to a change of parameters, as shown in Table 2. Here, s_G is a scaling factor with which $\hat{G}$ is multiplied; a value smaller than one implies a larger effect and hence more of an oscillation suppression. Note that only a limited study on the variation of the parameters has been performed. A more detailed analysis will be carried out in the final version of the paper.

The resulting response for the flexible launcher with engine dynamics and slosh is shown in Figs. 12 and 13. It is clear from the comparison with Figs. 8 and 9 that the response has improved a lot, and most oscillations have been removed from the swivel command. Also the slosh motion is slower, although a small oscillation in the slosh states remains, due to a lack of damping. This could possibly reduced by further optimising the controller design. The first flexible mode is coupled to the slosh modes, as a similar oscillation can be observed in the flexible "position". However, also a small-amplitude vibration in the "velocity" is observed for the case with turbulence, which will hopefully be reduced once a proper navigation filter is

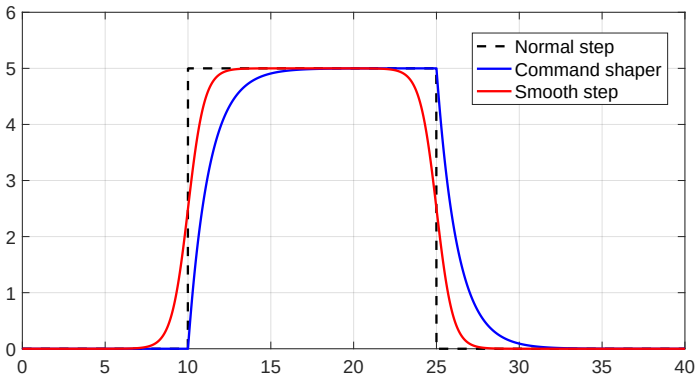

Figure 11. Difference between normal block function, block with command shaper, and a smooth block function. Differences have been exaggerated.

Table 2. INDI-SMC design-parameter update.

Parameter	Old value[7]	New value
$\mathbf{C}$	$\begin{bmatrix}1 & 8 & 0 & -0.06 & 0 & -0.03\end{bmatrix}$	$\begin{bmatrix}1 & 9.95 & 0 & -0.075 & 0 & -0.037\end{bmatrix}$
ρ	0.80	0.99
k_1	5.00	2.53
k_2	5.00	4.18
s_G	1.00	0.81

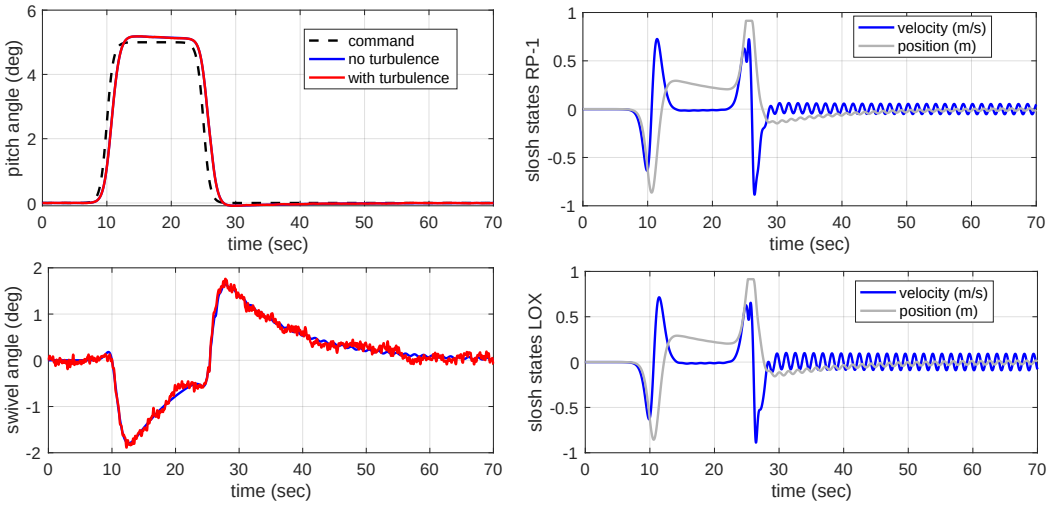

Figure 12. Full-model response with relaxed step command and updated controller: pitch response and swivel angle.

designed.

A final response test is done by changing the step input. In the previous test, the sigmoid function, Eq. (26), was applied with $a = 2$. Reducing this to $a = 1$ gives the results shown in Fig. 14. The slosh states behave very well now, and the undamped oscillation from before is gone (note that the case without turbulence is shown). When gust/turbulence is encountered, then naturally the rigid-body motion and the sloshing motions are both excited in the open-loop case. By contrast, with the closed-loop controller presented in this paper, the rigid-body and sloshing dynamics are damped and smoothened, by virtue of the active anti-disturbance actions of the control input. This phenomenon has also been seen in previous

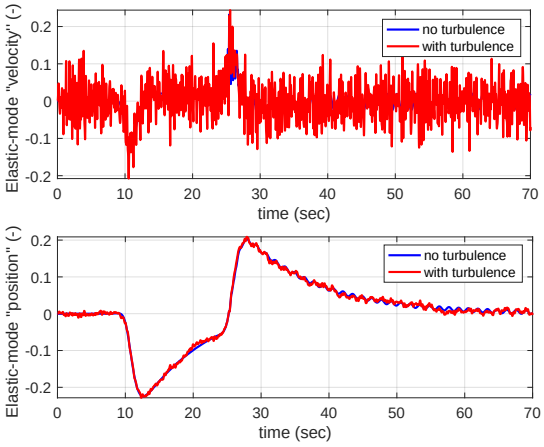

Figure 13. Full-model response with relaxed step command and updated controller: first flexible mode.

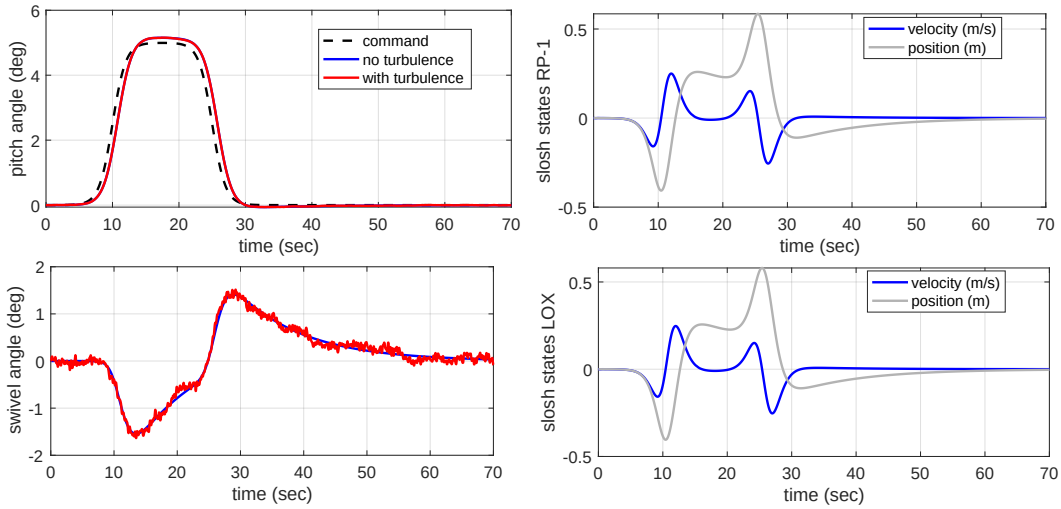

Figure 14. Full-model response with relaxed step command.

disturbance rejection research of nonlinear incremental control.[16] This result also shows the need to reflect on the manner how the guidance commands are issued. In case no mechanical means are present to damp the slosh motion, this may a good solution to avoid potential control problems.

V. Rigid-State Observer Design

The slosh observer as applied above[6] works very well, provided that there is sufficiently accurate knowledge about the rigid-body states, most notably the pitch angle and pitch rate. These two parameters are also fed back to the INDI-SMC, thus the development of a rigid-state observer seems to be the next logical step. This development is briefly discussed here, and is part of on-going research. Note that the addressed changes discussed earlier (smooth step input, feedback filters) have been included where appropriate.

The rigid-body part of the complete system is by nature a linearised version of the system dynamics. Therefore, to explore filtering techniques it makes sense to begin with a very basic state estimator, *i.e.,* the linear Kalman filter. In terms of sensor measurements, it is currently assumed that the rigid-body state is available through noisy measurements. No sensors have yet been modelled, and even though we are aware of this limitation, the current exercise will show first stability of the controlled system, including engine dynamics, sloshing, flexible modes, and input errors due to the use of rigid-body and slosh-state observers. The applied noise is normally distributed white noise with $1\sigma = 0.18^\circ$ for α and θ and $0.018^\circ/\text{s}$ for q.

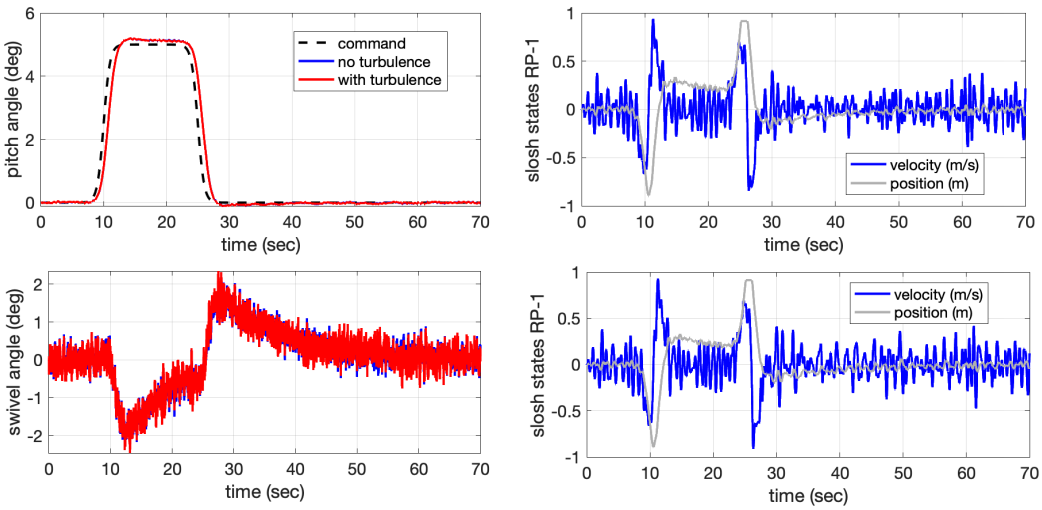

Figure 15. Filtering of rigid-body states with a linear Kalman filter: pitch angle, swivel angle and slosh states.

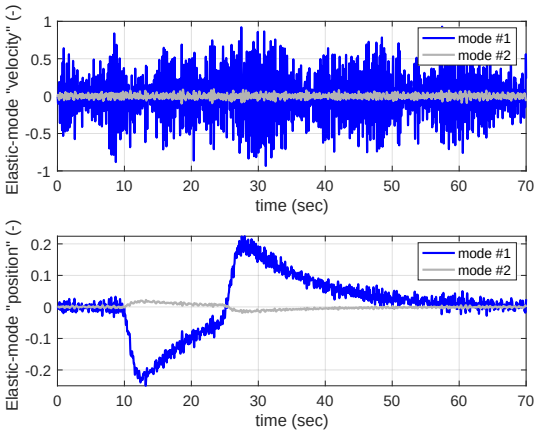

Figure 16. Filtering of rigid-body states with a linear Kalman filter: elastic-body states.

Using the Kalman-filter output as input to the controller, including a pitch acceleration differentiated from the estimated (noisy) pitch rate, the results as shown in Figs. 15 and 16 are obtained. These are obviously not the ideal results, but they serve as indication that the loop can indeed be closed for a very complex model with many different dynamics effects, as well as two state observers and a vehicle embedded in a turbulent wind field. The pitch response shows that the pitch angle is actually accurately captured. However, the swivle angle exhibits a very noisy behaviour, due to the effect of noisy measurements and the turbulent wind field. The slosh states, though, do not shown any wildly oscillating behaviour, and do not seem to destabilise the overal motion. The same can be said of the elastic-body states, although the vibrational effect is quite a bit stronger compared to the response shown in Fig. 13. Finally, in Fig. 17 the "estimation error", *i.e.,* the difference between the propagated rigid-body state and their estimated values, is shown. This is typically the error that is fed back to the controller.

All mentioned aspects have to be addressed in a more formal way, of course, but this only makes sense when the modelling is taken to the next level: modelling the dynamics as a fully non-linear system, including sensor dynamics with realistic error models, and a filter that will fuse the data from different sensors. This will indeed be the focus of the next steps in the research.

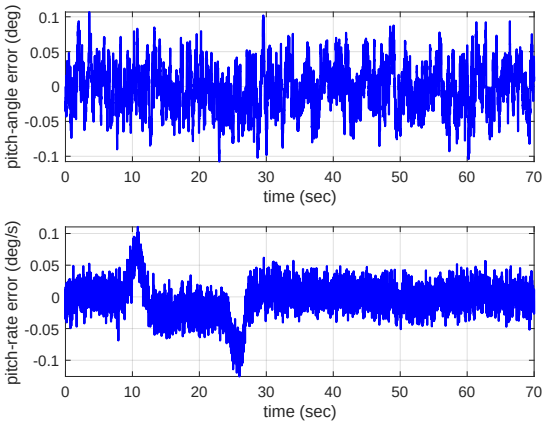

Figure 17. Filtering of rigid-body states with a linear Kalman filter: state error (= real - estimated state).

VI. Conclusions and Recommendations

This paper focuses on the attitude-tracking problem of a launch vehicle with propellant slosh in a turbulent atmosphere. Two controllers are designed and compared for this objective: a PD controller and an Incremental Non-Linear Dynamic Inversion Sliding Mode Controller (INDI-SMC). First, their performance is compared in a rigid-body tracking problem in the presence of atmospheric turbulence. When a five-degree pitch angle step command is given, the PD controller presents around 10% of overshoot, while the INDI-SMC shows much smaller tracking errors. However, its capability to remove turbulence induced oscillations from the swivel commands appeared to be limited. Therefore, various filter designs have been implemented to improve the smoothness of INDI-SMC control. Using either a notch or band-pass filter in the sensor-feedback loops of pitch angle and pitch rate only marginally reduced the swivel oscillations, but did not solve the problem.

Since the INDI-SMC design has shown superior performance on the rigid-body command tracking task, its effectiveness on an aeroelastic launcher with propellant slosh was tested next. Simulation results show that in this circumstance, INDI-SMC itself experiences diverging oscillatory behaviour, which can be successfully suppressed by including band-pass filters in the sensor feedback loops for the pitch angle and rate. The (sub-optimal) cut-off frequency of the band-pass filters was selected from Monte-Carlo simulations. Moreover, due to the coupling effects between rigid body, engine, sloshing, and aeroelastic dynamics, step commands in the pitch angle result in spikes in slosh states and swivel angles. Despite these strong couplings, the INDI-SMC method can execute the tracking command while rejecting disturbances.

When more realistic engine dynamics are simulated, a change of values of the controller design parameters is required. However, once done, a robust response is obtained. Changing the step input to a sigmoid function also helps to reduce the oscillations of the slosh states. A preliminary rigid-body state estimator (linear Kalman filter) has been included in the feedback loop to the controller, assuming noisy measurements of the rigid-body states. Running the complete system, including engine dynamics, sloshing, flexible modes, and input errors due to the use of rigid-body and slosh-state observers, shows that the controller remains stable at all times, even though the swivel input has become very noisy. All observed limitations have to be addressed in future work, but only when the modelling of dynamics and sensors is taken to the next level of complexity (and realism).

Although the control method presented in this paper is nonlinear, the simulation model of the aeroelastic launch vehicle with propellant slosh adopted in this paper is still linear. Future work will focus on modelling the fully-coupled nonlinear dynamics and further validate the performance and robustness of the nonlinear controller on the developed nonlinear platform. Then, also all design changes will be brought together and the controller design will be reoptimised.

References

[1]Lester, H.C. and Collins, D.F., "Determination of Launch-Vehicle Response to Detailed Wind Profiles", AIAA-64-82, *Aerospace Sciences Meeting*, New York, NY, 1964.

[2]Meirovitch, L., and Wesley, D. A., "On the Dynamic Characteristics of a Variable-Mass Slender Elastic Body Under High Accelerations", *AIAA Journal*, Vol. 5, No. 8, 1967, pp. 1439-1447.

[3]Geissler, E.D., "Wind Effects on Launch Vehicles", AGARDograph No. 115, 1970.

[4]Mooij, E. and Gransden, D. I., "The Impact of Aeroelastic Effects on the controllability of Conventional Launch Vehicles", *Proceedings of the 67th IAC Conference*, Guadalajara, Mexico, September, 2016.

[5]Mooij, E. and Gransden, D. I., "Quasi-Transient Stability Analysis of a Conventional Aeroelastic Launch Vehicle", *Proceedings of the 68th IAC Conference*, Adelaide, Australia, September 25-29, 2017.

[6]Mooij, E., "Slosh Observer Design for Aeroelastic Launch Vehicles", AIAA-2020-1606, *AIAA SciTech Forum, Guidance, Navigation, and Control Conference*, Orlando, Florida, 6-10 January 2020.

[7]Mooij, E., and Wang, X., "Incremental Sliding Mode Control for Aeroelastic Launch Vehicles with Propellant Slosh", *AIAA Scitech 2021 Forum*, Virtual Conference, January 11-21, 2021.

[8]Wang, X., Sun, S., van Kampen, E., and Chu, Q., "Quadrotor Fault Tolerant Incremental Sliding Mode Control driven by Sliding Mode Disturbance Observers", *Aerospace Science and Technology*, Vol. 87, pp. 417-430, 2019.

[9]Fleeter, R., Mcloughlin, F. and Mills, R., "A Low-Cost Expendable Launch Vehicle for 500-Pound Class Satellites", Marketing brochure, PacAstro, Herndon, VA, 26 May 1992.

[10]Mooij, E. and Gransden, D.I., "The Effect of Sloshing on the Controllability of a Conventional Aeroelastic Launch Vehicle", AIAA-2019-0116, *AIAA SciTech Forum, Guidance, Navigation, and Control Conference*, San Diego, CA, 5-9 January 2019.

[11]Abramson, H.N., "The dynamic behavior of liquids in moving containers: with applications to space vehicle technology", NASA SP-106, 1966.

[12]Abramson, H.N., Chapter 8, "Liquid Propellant Dynamics", in: Mazet, R., *Manual on Aeroelasticity*, Volume I, AGARD Report R-578, 1968.

[13]Department of Defense, "Flying Qualities of Piloted Airplanes", MIL-F-8785C, Nov. 5, 1980.

[14]Justus, C.G., Campbell, C.W., Doubleday, M.K., and Johnson, D.L., "New Atmospheric Turbulence Model for Shuttle Applications", NASA TM-4168, January 1990.

[15]Wang, X., van Kampen, E., Chu, Q., and Lu, P., "Stability Analysis for Incremental Non-linear Dynamic Inversion Control", Journal of Guidance, Control, and Dynamics, Vol. 42, No. 5, 2019, pp. 1116–1129.

[16]Wang, X., Mkhoyan, T., Mkhoyan, I., and De Breuker, R., "Seamless Active Morphing Wing Simultaneous Gust and Maneuver Load Alleviation", Journal of Guidance, Control, and Dynamics, Vol. 44, No. 9, 2021, pp. 1649-1662.

[17]Yu, S., Yu, X., Shirinzadeh, B., and Man, Z., "Continuous finite-time control for robotic manipulators with terminal sliding mode", *Automatica*, Vol. 41, No. 11, 2005, pp. 1957–1964.

[18]Mooij, E., "Robust Control of a Conventional Aeroelastic Launch Vehicle", AIAA-2020-1103, *AIAA SciTech Forum, Guidance, Navigation, and Control Conference*, Orlando, Florida, 6-10 January 2020.

Appendix A. Controller Performance Indices

To compare the controller responses and the effect of sloshing, several performance metrics will be defined. The first one is the minimum attitude deviation of the launcher with respect to the guidance commands, whereas the second one is the swivel effort that is required to achieve this. These two objectives can be expressed as the integrated pitch-angle deviation and the integrated swivel angle (equivalent to, for instance, the total hydraulic power required), given by:

$$\sum_{\theta_{err}} = \int_0^{\mathrm{T}} |\theta_c(t) - \theta_p(t)| \mathrm{d}t \qquad \sum_{\varepsilon_T} = \int_0^{\mathrm{T}} |\varepsilon_T(t)| \mathrm{d}t \tag{27}$$

A graphic representation of the above metrics is shown in Fig. A1(a), represented by the grey areas, for a 2° step command in θ, starting at $\Delta t = 1$ s with a duration of 14 s. For optimal controller performance, both individual areas should be as small as possible, which means that their numerical equivalent can be used to evaluate different controller designs. In the given example, $\sum_{\theta_{err}} = 6.55°\text{s}$ and $\sum_{\varepsilon_T} = 17.21°\text{s}$.

Another metric can be the oscillatory behaviour of either state or control variable. Oscillations in the control may not only be energy expensive and a burden on the hardware, it could also lead to instabilities. Equivalently, oscillations in the slosh states gives an indication of the severity of the motion and potential hazardous situations. To detect oscillations or otherwise discrete changes in the controls, the cumulative moving standard deviation can be used. For a subset j of n_s out of a total of N samples of an arbitrary control signal u, the moving mean is defined as $\bar{y}_j = \frac{1}{n_s} \sum_{i=j}^{j+n_s-1} u_i$. Here, j will run from $j = 1+n_s/2$ to N-$n_s/2$, so each subsequent subset will shift by only one sample. Let the squared deviation from this mean be defined as $s_{u,j} = (u_{j+n_s/2} - \bar{y}_j)^2$, which represents the value at the midpoint of subset j. The cumulative standard deviation, F_u, for subset j is then

$$F_{u_j} = \sqrt{\frac{1}{N - n_s - 1} \sum_{k=1}^{j} s_k} \tag{28}$$

As an example, in Fig. A1(b) the oscillation pattern of the slosh velocity is shown, due to a poorly designed control system. The cumulative standard deviation increases more rapidly when a discrete jump occurs, or when there is an interval with persistent oscillations. As a metric, the grey area under the curve can be used, which, while minimised, would lead to a smoother behaviour. In this particular example, the numerical value is $F_{z_s} = 35.6$ m/s.

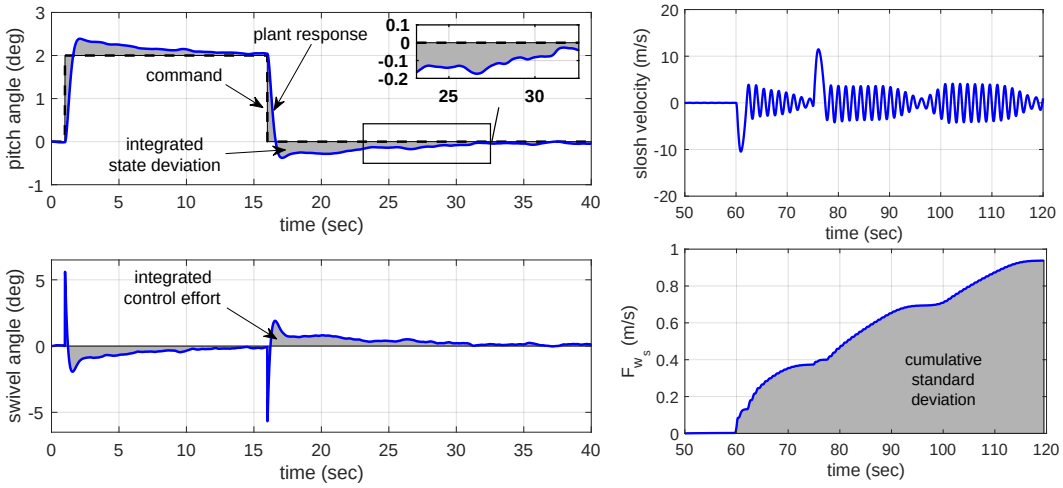

(a) State deviation and control effort

(b) Oscillatory behaviour

Figure A1. Controller performance indices.